15 December 1995

ELSEVIER

Chemical Physics Letters 247 (1995) 142–148

CHEMICAL PHYSICS LETTERS

Dynamics of hydrogen bonding and energy transfer in matrix-assisted laser desorption

Akos Bencsura [a], Akos Vertes [b]

[a] *Department of Chemistry, The Catholic University of America, Washington, DC 20064, USA*
[b] *Department of Chemistry, The George Washington University, Washington, DC 20052, USA*

Received 30 September 1995

Abstract

A molecular dynamics simulation of matrix-assisted laser desorption is presented for host and guest particles with internal structure. The laser-induced phase transition is modeled in a hemispherical volume of pyridine-3-carboxylic acid matrix seeded with a leucine enkephalin guest molecule. Following an instantaneous temperature jump to 1500 K, representing the laser excitation, the network of hydrogen bonds is disrupted in approximately 3 ps. After a 0.7 ps segregation period, the guest molecule is entrained by the evaporating matrix molecules. The guest lift-off velocity is estimated at ≈ 156 m/s, a value about a factor of two lower than measured for neutral matrix molecules in similar systems.

1. Introduction

Matrix-assisted laser desorption ionization (MALDI) in combination with mass spectrometry has become an important tool in bio- and synthetic polymer characterization [1–3]. Protein molecules with masses exceeding 200000 amu can be volatilized using MALDI. The most commonly utilized variant of the method is based on embedding the guest molecules (proteins, nucleic acids, synthetic polymers, etc.) into crystals of relatively small organic molecules (matrix). This step is followed by laser-induced coevaporation and ionization of matrix and guest molecules. As pointed out by two recent reviews, despite the substantial success of MALDI for the gas phase spectroscopy of large molecules, the theoretical description of its mechanism is legging behind [3,4].

Earlier attempts to deal with certain aspects of the MALDI process included a kinetic model of energy repartitioning ('homogeneous bottleneck model') [5,6] based on the concept of selective bond breaking [7], a pressure pulse model [8], a hydrodynamic model of plume expansion ('cool plume model') [9], and a molecular-dynamics (MD) simulation of bulk desorption based on the hard sphere representation of all particles [10]. Related MD studies of cluster desorption from solid surfaces [11] and atom ejection from high-energy ion tracks [12] revealed the conceptual similarity between other fast desorption experiments and MALDI. Although these models are able to account for several features of the MALDI experiment, none of them has attempted to describe the contributions made by the internal structure of host and guest molecules. The generally observed extensive fragmentation of matrix molecules, and lack of fragmentation or moderate metastable decay for the guest molecules obviates the need to account for the internal degrees of freedom.

Due to the high demand for information on pro-

SSDI 0009-2614(95)01179-X

tein folding and active site dynamics in aqueous environment a growing number of MD codes is available to describe conformational changes of macromolecules embedded in an environment of small molecules [13]. These MD codes, e.g. chemistry at Harvard molecular mechanics (CHARMM), rely on the atom- and group-based treatment of nonbonded interactions between the macromolecule and its molecular environment [14]. To reduce the number of required interactions the CHARMM program makes use of the so-called 'extended-atom representation', whereby certain hydrogens of the macromolecule are combined with the neighboring heavy atoms. This simplification substantially reduces the number of required pair potentials, while retains many important features of the polypeptide backbone and side groups. Recent applications of the CHARMM code include the simulation of proteins both in crystal [15] and in aqueous environments [16].

Our objective is to enhance the understanding of cocrystallization and coevaporation in the MALDI method at the microscopic level by exploiting these MD codes for the description of peptide–matrix systems. As a departure from the MD of hard spheres [10], both the matrix and the guest molecule can be represented by their detailed structure based on crystallographic data. In the present communication the CHARMM code is used to model the network of hydrogen bonds between host molecules, the host–guest interactions in the embedding process, and the crystal dynamics upon laser excitation. A major simplification in this approach is the neglect of fragmentation and ionization processes. Although these omissions limit comparisons with mass spectrometric data, they are necessary in order to keep the number of included interactions at manageable level. To the best of our knowledge, this work is the first attempt to account for the effect of molecular structure and internal degrees of freedom in the MALDI process.

2. Methods of calculation

The MD calculations were carried out with a recent version of CHARMM (Versions c22g5 and c23f4) [14]. During the simulations, only polar hydrogen atoms were represented explicitly, nonpolar groups were modelled as extended atoms. The empirical potential energy function consisted of bond stretching and bending, dihedral, improper, electrostatic, and van der Waals energy terms. No explicit hydrogen bonding term was used. The forces stemming from the nonbonding interactions were smoothly switched to zero between 800 and 1200 pm [16]. Both the selected matrix, pyridine-3-carboxylic acid (nicotinic acid), and the guest molecule, leucine enkephalin (Tyr–Gly–Gly–Phe–Leu), were represented by their detailed molecular structure.

There were two departures from the regular macromolecular simulations in CHARMM: the introduction of a nonaqueous medium (matrix), and the onset of a temperature jump (representing the laser heating) leading to phase transition. The parameters for the amino acid residues and in part for the new medium, nicotinic acid, were taken from the parameter file of the CHARMM program. Missing parameters for the nicotinic acid were estimated by analogy. Wave functions and charge distributions of the nicotinic acid molecule were calculated using the GAMESS ab initio program for the fully optimized structure at the 3-21G* level [17]. The CHelpG feature of the GAMESS program provided electrostatic potential derived atomic charge distributions [18].

To simplify and accelerate the MD calculations of the solid–vacuum interface, spherical boundary conditions were used. A hemisphere of the nicotinic acid matrix with a maximum diameter of 4800 pm was constructed using the X-ray based crystallographic structure determined by Wright and King [19]. In order to establish the initial matrix coordinates for the simulation the unit cell was repeated six times in all three directions. From this block a sphere was cut out by deleting all molecules that were entirely outside a radius of 2200 pm from the origin. Finally, all the molecules with positive y coordinates were deleted. This procedure resulted in a hemisphere with 2300 pm average radius containing 202 nicotinic acid molecules. Initially the structure was energy minimized, and a fully extended leucine enkephalin molecule was incorporated into the matrix. At insertion the backbone of the peptide was aligned parallel to the rings of the nicotinic acid matrix [20]. The center of mass of the peptide molecule was 250 pm below the surface of the

matrix. In preparation for the dynamics simulation the whole structure was energy minimized again with 200 steps of steepest descent and 200 steps of adopted basis set Newton–Raphson method.

The stochastic boundary molecular dynamics method was used for the desorption simulations [21]. The previously described hemisphere was divided into three regions. The reaction region contained all atoms within a 1900 pm radius sphere. Atoms between 1900 and 2200 pm made up the buffer region and atoms beyond 2200 pm the reservoir region. Movement of the atoms in the buffer and reservoir regions were restrained by a 0.084 kJ/mol pm (2.0 kcal/mol Å) harmonic force. The reaction region and the flat surface of the hemisphere were unrestrained throughout the simulation. A uniform 200 ps^{-1} frictional coefficient was employed on all heavy atoms in the buffer region. The dynamics equations of motions were numerically integrated with the leap-frog integrator with 1 fs time step.

To observe the room temperature structure in the presence of the peptide, the previously energy minimized system was equilibrated at 300 K for 45 ps. After the completion of the 300 K simulation, the temperature of the matrix was increased by instantaneously scaling the velocities of atoms in the nicotinic acid. This sudden increase of temperature simulated the laser excitation of the matrix. Another 45 ps dynamics production run was performed to explore the events following the laser pulse. The coordinates and velocities of all the particles were saved at every 100th step for later analysis. All the calculations were carried out on Indigo and Indigo^2 workstations (Silicon Graphics, Mountain View, CA). Molecular trajectories were visualized and animated by the SCARECROW package (Centre for Scientific Computing, Espoo, Finland) obtained from the public domain.

3. Results and discussion

The validity of the interaction potentials was tested by comparing the equilibrated 300 K crystal structure of nicotinic acid to the original X-ray diffraction data. Intramolecular bond lengths and angles were essentially unaltered, whereas the intermolecular hydrogen bond between the pyridine nitrogen and the carboxyl oxygen expanded by about 10% from the measured 266 pm to 300 pm. It is interesting to note that the well-known pairing of carboxylic acid molecules via the formation of two hydrogen bonds between the carboxyl groups is absent in both the experimental and the calculated structure of nicotinic acid. Instead, chains of nicotinic acid molecules with similar orientation form a layered structure with the neighboring chains facing in opposite directions. Substantial departures from the X-ray based structure are observed at the hemispherical boundary, where the symmetry of the molecular environment is broken.

To further test the adequacy of the interaction potentials, the energy of sublimation was calculated by comparing the energy of the system before and after a nicotinic acid molecule was detached from the solid phase: $\Delta E_{sub}(\text{calc}) = 101.5$ kJ/mol. Thus, at 300 K the calculated molar enthalpy of sublimation ($\Delta H_{sub}(\text{calc}) = 104.0$ kJ/mol) agreed within experimental error with the measured value ($\Delta H_{sub}(\text{exp}) = 104.6$ kJ/mol). This remarkably good – probably fortuitous – agreement is especially relevant to our simulation because the matrix volatilization involves the transfer of numerous molecules from the solid to the gas phase.

Upon the 300 K equilibration, after the insertion of leucine enkephalin molecule into the matrix crystal, a substantially stressed structure developed. In the vicinity of the guest molecule the host particles were tilted and displaced (see Fig. 1a). During the equilibration phase, however, the guest molecule retained its preferential embedding along the layered structure of the host crystal. This observation seems to be in accordance with the conclusions of dye tagging studies of protein embedding into the matrix crystal [20]. The 300 K equilibration phase of the calculation also has some relevance to sample preparation, one of the critical steps in MALDI. The basis of the best established sample preparation method is fast cocrystallization of matrix and guest molecule from their saturated solution [20]. In this highly non-equilibrium process the guest molecules may be entrapped in the matrix crystals leading to configurations similar to the one depicted in Fig. 1a. Future analysis of equilibrated structures involving different matrices and different peptides may lead to better understanding of the embedding process.

The laser-generated volatilization of matrix crystals is believed to be at the core of the MALDI process [22]. The energy deposition by the laser was modeled by introducing vibrational excitation to the atoms of the matrix. Assuming UV laser irradiation, this can be viewed as a consequence of electronic excitation followed by internal conversion, whereas, in the case of an IR laser source, the vibrational

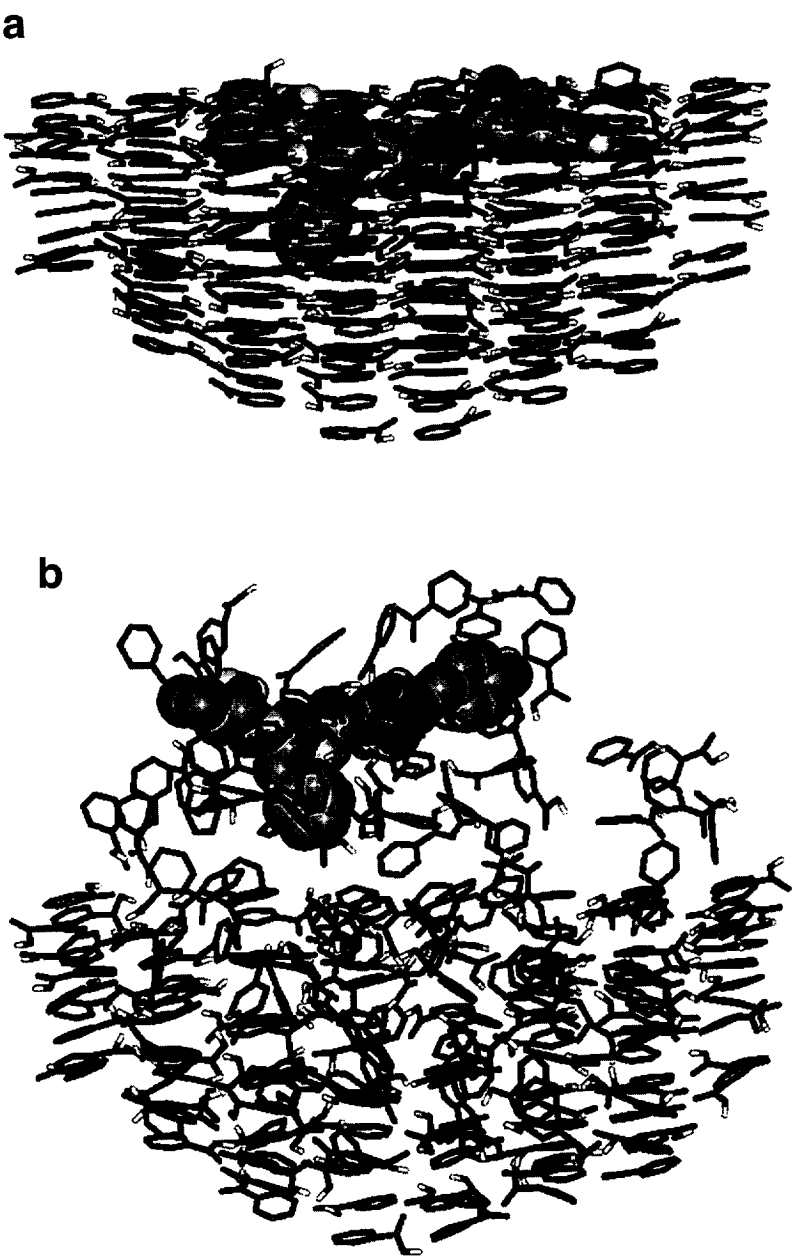

Fig. 1. MD simulation of MALDI in a hemisphere of 4800 pm diameter. The leucine enkephalin guest molecule is embedded in nicotinic acid matrix. (a) Equilibrium configuration is shown at 300 K. (b) Adiabatic temperature jump to 1500 K leads to the expulsion of the guest molecule. At 3 ps the guest molecule lifts off accompanied by several matrix molecules. At this stage the peptide has clearly detached from the surface and the number of accompanying matrix molecules has dropped.

modes are excited directly. There is no data on the transient internal temperature of matrix molecules immediately after the laser pulse. A rough estimate of the deposited energy with the assumption of about 50% conversion rate leads to ≈ 1500 K internal temperature. Although this assumption was highly arbitrary, calculations using other temperatures led to qualitatively different results that did not describe the experimental findings. For example, at 900 K no noticeable evaporation took place on the picosecond timescale, whereas at 2800 K the model system virtually exploded. Thus, in order be able to trace the volatilization on the picosecond timescale with our MD simulation, we decided to use 1500 K.

After the equilibration at 300 K the temperature in the simulation was switched to 1500 K. In about 3 ps the matrix crystal underwent phase transition and vigorous evaporation of nicotinic acid molecules was observed at the surface (Fig. 1b). More interestingly, in about 0.7 ps the guest molecule floated to the surface of the host crystal. This phenomenon, known as radiation-induced segregation, is due to the reduced strain and lower potential energy associated with the surface position of this apolar peptide. After the relaxation/segregation period, more matrix evaporated and the peptide molecule was entrained.

To compare the matrix structure before and after the excitation, pair correlation functions (PCF), $g(r)$, were calculated between certain atoms. The statistical analysis showed dramatic changes in the normalized PCFs (Fig. 2). At 300 K the N–O1 PCF describing the correlation between the O in the carboxyl OH

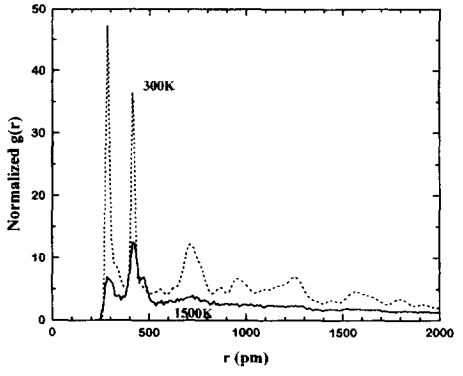

Fig. 2. Normalized pair correlation functions between the pyridine N and the O in the carboxyl OH at 300 K (45 ps average) and after the temperature jump to 1500 K (10 ps time stage).

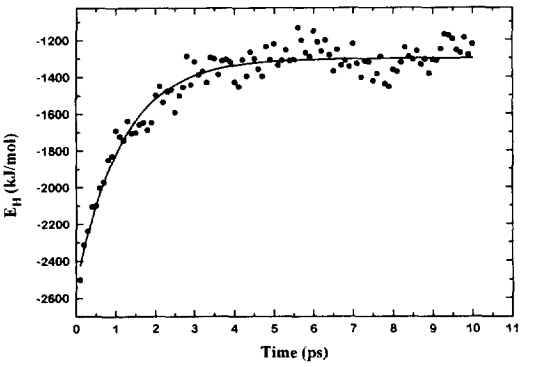

Fig. 3. Time dependence of the energy associated with hydrogen bonds in nicotinic acid after an adiabatic temperature jump from 300 to 1500 K.

and the pyridine N exhibited two sharp maxima at 300 and 410 pm. These peaks corresponded to the hydrogen bond and to the intramolecular correlation between N and O1, respectively. The four additional peaks on the normalized $g(r)$ function indicate long-range order in the nicotinic acid crystal. Almost the entire contribution related to the hydrogen bonds disappeared at 1500 K. Although the increased vibration broadened the peak, a relatively large portion of the intramolecular N–O1 correlation was preserved. However, all the peaks related to long-range order in the crystal disappeared. The breakdown of both short- and long-range order indicates that due to the laser heating the matrix crystal undergoes transient local melting before evaporation. This is counterintuitive compared to the macroscopic observation of a sublimation-like process.

It is possible in the calculation to separate the energy associated with hydrogen bonds from the total energy of the system. We have to emphasize that the interaction potentials do not contain explicit hydrogen bonding contributions. Thus, the hydrogen bonding energies were not a priori part of the model. The energy associated with hydrogen bonds, E_H, was followed throughout the simulation. Due to the fast breakup of the crystal structure after the temperature jump, E_H dropped precipitously and, in about 3 ps, reached its new steady state value (see Fig. 3). It is worthwhile to note that due to the boundary condition a substantial part of the crystal did not evaporate and about half of the cohesive energy remained unchanged. This limitation may be an indi-

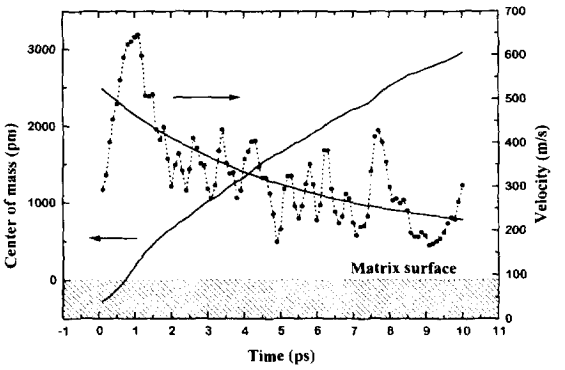

Fig. 4. Perpendicular component of the position and center-of-mass velocity of the leucine enkephalin molecule measured from the nicotinic acid surface as a function of time after the excitation.

cation that larger scale simulation is needed for more accurate results.

The fate of the peptide molecule was followed by recording the position and velocity of its center of mass relative to the matrix surface (Fig. 4). Initially, the guest molecule is buried ≈ 250 pm below the surface. After the temperature jump its velocity surges to about 600 m/s and in about 0.7 ps the leucine enkephalin molecule emerges at the surface. This is the segregation phase mentioned earlier in the discussion. In the next desorption phase, the guest molecule lifts off while its velocity shows exponential decay with a decay time of ≈ 6 ps and a limiting value of ≈ 156 m/s. During this process the number of attached matrix molecules drops together with the number of collisions between the matrix and guest molecules. The number of attached matrix molecules does not necessarily go to zero, as it is demonstrated by the observation of matrix adducts in MALDI mass spectra [3].

The limiting velocity of the guest molecule can be compared to earlier hydrodynamic calculations [9] and velocity distribution measurements [23]. One-dimensional hydrodynamics calculations on frequency-quadrupled Nd:YAG laser excitation (266 nm, 10^7 W/cm^2) of ferulic acid matrix indicated 250 m/s for the drift velocity of the plume center of mass at 40 ns. In the corresponding experiments, under similar conditions, the measured neutral velocities for the ferulic acid matrix exhibited maxima between 300 and 400 m/s [23]. Since they are on three different time scales one has to exercise caution when comparing the three different velocities. The limiting velocity values from MD simulations are determined on the picosecond scale, while the hydrodynamic velocities typically become meaningful on the nanosecond time scale. Neutral velocity measurements are usually based on post-ionization measurements applying a delayed second laser pulse for ion generation. The delay times involved in these experiments may be in the hundreds of nanosecond range. In addition, the magnitude of the temperature jump in the MD simulation can also influence the velocity values. Therefore, direct comparison of the velocities from the three different sources has to be taken with caution.

References

[1] K. Tanaka, H. Waki, Y. Ido, S. Akita, Y. Yoshido and T. Yoshida, Rapid Commun. Mass Spectry. 2 (1988) 151.
[2] F. Hillenkamp, M. Karas, R. Beavis and B.T. Chait, Anal. Chem. 63 (1991) 1193A.
[3] A. Vertes and R. Gijbels, in: Laser ionization mass analysis, eds. A. Vertes, R. Gijbels and F. Adams (Wiley, New York, 1993) p. 127.
[4] R.E. Johnson, in: Large ions: their vaporization, detection and structural analysis, ed. T. Baer (Wiley, Chichester, 1995) in press.
[5] A. Vertes and R.D. Levine, Chem. Phys. Letters 171 (1990) 284.
[6] A. Vertes, R. Gijbels and R.D. Levine, Rapid Commun. Mass Spectry. 4 (1990) 228.
[7] R.N. Zare and R.D. Levine, Chem. Phys. Letters 136 (1987) 593.
[8] R.E. Johnson, Int. J. Mass Spectrom. Ion Processes 139 (1994) 25.
[9] A. Vertes, G. Irinyi and R. Gijbels, Anal. Chem. 65 (1993) 2389.
[10] J. Shiea and J. Sunner, in: Methods and mechanisms for producing ions from large molecules, eds. K.G. Standing and W. Ens (Plenum Press, New York, 1991) p. 147.
[11] T.A. Holme and R.D. Levine, Surface Sci. 216 (1989) 587.
[12] H.M. Urbassek, H. Kafemann and R.E. Johnson, Phys. Rev. B 49 (1994) 786.
[13] K.B. Lipkowitz and D.B. Boyd, eds., Reviews in computational chemistry, Vol. 6 (VCH Publishers, Weinheim, 1995) Appendix 2.
[14] B.R. Brooks, R.E. Bruccoleri, B.D. Olafson, D.J. States, S. Swaminathan and M. Karplus, J. Comput. Chem. 4 (1983) 187.
[15] A.M. Micu, D. Durand, M. Quilichini, M.J. Field and J.C. Smith, J. Phys. Chem. 99 (1995) 5645.

[16] P.J. Steinbach and B.R. Brooks, J. Comput. Chem. 15 (1994) 667.
[17] M.W. Schmidt, K.K. Baldridge, J.A. Boatz, S.T. Elbert, M.S. Gordon, J.J. Jensen, S. Koseki, N. Matsunaga, K.A. Nguyen, S. Su, T.L. Windus, M. Dupuis and J.A. Montgomery, J. Comput. Chem. 14 (1993) 1347.
[18] C.M. Breneman and K.B. Wiberg, J. Comput. Chem. 11 (1990) 361.
[19] W.B. Wright and G.S.D. King, Acta Cryst. 6 (1953) 305.
[20] R.C. Beavis and J.N. Bridson, J. Phys. D 26 (1993) 442.
[21] A. Brünger, C.L. Brooks III and M. Karplus, Proc. Natl. Acad. Sci. US 82 (1985) 8458.
[22] W. Ens, Y. Mao, F. Mayer and K.G. Standing, Rapid Commun. Mass Spectry. 5 (1991) 117.
[23] T. Huth-Fehre and C.H. Becker, Rapid Commun. Mass Spectry. 5 (1991) 378.